Electronic Supplementary Information (ESI)

A zeolite-like MOF based on a heterotritopic linker of imidazolyl, carboxyl and pyridine with a long-sought uks net on Schwarz's *D*-surface

Chun-Rong Ye, Ji Zheng, Mian Li* and Xiao-Chun Huang*

Department of Chemistry and Key Laboratory for Preparation and Application of Ordered Structural Materials of Guangdong Province, Shantou University, Guangdong 515063 (China).

**E-mail: mli@stu.edu.cn (M.L.); xchuang@stu.edu.cn (X.C.H.)*

Experimental section:

Materials

All analytical grade chemicals such as 2,3-diaminobenzoic acid ($C_7H_8N_2O_2$, 98%), 4-pyridinecarboxaldehyde (C_6H_5NO, 99%), *N*,*N*-dimethylformamide (C_3H_7NO, 99%) etc, were purchased from commercial sources and used without further purification.

Synthesis of ligand {2-(pyridin-4-yl)-1*H*-benzo[d]imidazole-7-carboxylic acid} (H_2L)

The ligand was synthesized by condensation reaction of 2,3-diaminebenzoic acid and 4-pyridinecarboxaldehyde. Firstly, 2,3-diaminobenzoic acid (40 mmol) was added to anhydrous *N*,*N*-dimethylformamide (100 mL). After mixing, 4-pyridinecarboxaldehyde (60 mmol) was added slowly and stirred overnight at 80 °C for 5 days. Precipitate was collected through decompression pumping device and washed with water several times. The ligand was recrystallized using a mixture of MeOH:H_2O (2:1). After 7 days, crystals of the ligand were washed with methanol and dried at 40 °C for 2 h to produce yellow block crystals around the yield (68%). The crystallographic data of the ligand was given in **Table S1**.

Elemental analysis (%) Calcd: C, 65.21; H, 3.76; N: 17.56. Found: C, 64.94; H, 3.79; N: 17.46. ^{1}H NMR (400 MHz, DMSO) δ 13.39 (s, 1H), 12.75 (s, 1H), 8.76 (d, J = 5.5 Hz, 2H), 8.29 (s, 2H), 8.00 (d, J = 7.6 Hz, 1H), 7.89 (d, J = 7.4 Hz, 1H), 7.38 (t, J = 7.8 Hz, 1H).

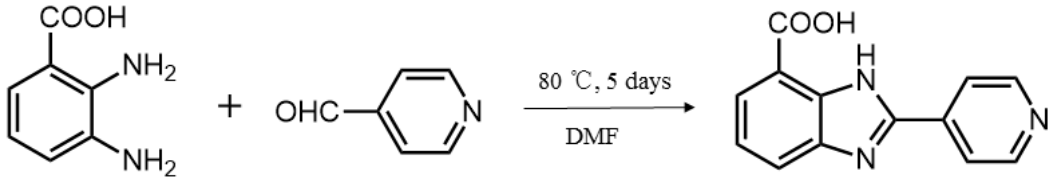

Fig. S1 Schematic representation of ligand synthesis.

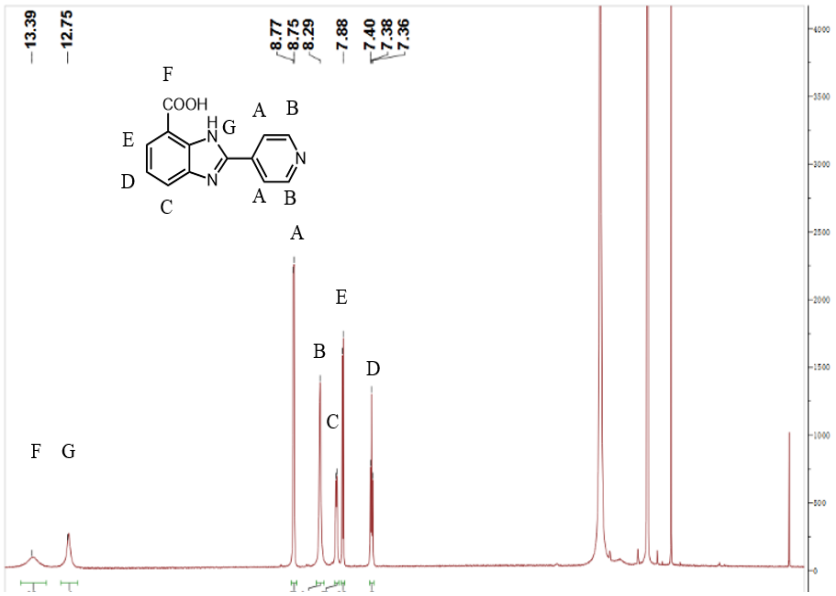

Fig. S2 ^{1}H NMR-spectrum of the ligand in DMSO.

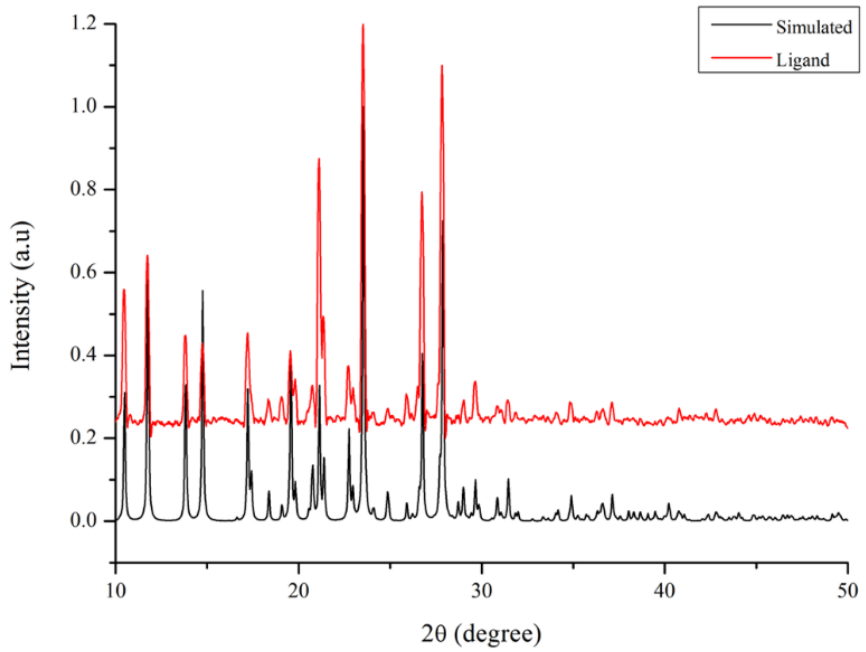

Fig. S3 Simulated and experimental PXRD patterns of the ligand.

Synthesis of YCR:

A mixture of H_2L (0.1 mmol), CuI (0.1 mmol), acetonitrile (4 mL), water (2 mL) and HNO_3 (0.2 mL) was sealed in a Teflon-lined stainless vessel (12 mL), heated at 120 °C for 10 h, and then cooled slowly to ambient temperature. The crystals were filtered and washed with methanol several times. Green cubic crystals were obtained with 78% yield based on H_2L. These crystals were soaked in methanol solution for 3 days prior to heating under vacuum at 100 °C for 12 h to obtain the guest free phase, labelled as **YCR′** and formulated as $\{[Cu_2(HL)_{1.6}(HL\text{-}I)_{0.4}NO_3]\cdot NO_3\}_n$. FT-IR (KBr, cm^{-1}): 3481(m), 1618(s), 1545(s), 1478(m), 1425(s), 1385(s), 1256(m), 1217(m), 1067(w), 1030(w), 838(m), 765(m), 622(w), 579(w), 533(w). See Fig. S5, S24-S26 for determination of chemical formula through additional characterizations.

Liquid-solid extraction experiments:

Single crystals of **YCR′** (20 mg) were immersed in aqueous solutions (0.01 mol/L) of NaN_3, NaSCN and $NaClO_4$ separately for 24 h at room temperature to yield anion exchanged products viz **YCR′**-N_3, **YCR′**-SCN and **YCR′**-ClO_4, respectively. After anion exchange, the products were washed with ultra-pure water several times and air dried, and then characterized by FT-IR, solid-state UV spectroscopy, TGA, PXRD and SEM analysis.

Anion exchange selectivity experiments:

Single crystals of **YCR′** (20 mg) were immersed in aqueous solutions (20 mL) of equimolar NaN_3 (0.2 mmol) and NaSCN (0.2 mmol) for 24 h at room temperature to yield the anion exchanged products. After anion exchange, the products were washed with ultra-pure water several times and air dried, and then characterized by FT-IR and PXRD. Similar anion exchange selectivity experiments were performed for N_3^-/ClO_4^-, SCN^-/ClO_4^- and $N_3^-/SCN^-/ClO_4^-$ mixtures.

Physical measurements:

FT-IR spectra were recorded on Nicolet Avatar 360 FT-IR spectrometer in the frequency range of 4000-400 cm^{-1} using KBr method. Powder X-ray diffraction patterns were obtained by using Cu K_α radiation (1.5418 Å) on a Rigaku D/M-2200T automated diffractometer. Elemental analyses

were obtained using Vario EL elemental analyzer. Thermogravimetric analyses were measured on a SHMADZU TA-50 thermal analyzer in the heating rate of 10 °C min^{-1} from RT to 800 °C under nitrogen gas flow. Morphological images were obtained using a JSM-6360LA scanning electron microscope. Gas adsorption measurements were recorded on a 3H-2000PS gas adsorption analyzer. Ion chromatography was measured from IC-1100 ion chromatograph.

X-ray crystallography:

A suitable crystal of **YCR** was carefully chosen under optical microscope and paste into the glass fiber for data collection at 100 K on a Bruker D8 Venture (operated at 25 kW power: 45 kV, 40 mA) using Cu K_α radiation (λ = 1.5418 Å). The structure was solved by direct methods and refined on F^2 using full-matrix least-squares technique (SHELXTL-97).[S1] All non-hydrogen atoms were refined anisotropically till convergence was reached. All the hydrogen atoms attached to organic moieties were generated geometrically. The crystallographic data of **YCR** was given in **Table S1**. Selected structural parameters of **YCR** were given in **Table S2.**

Table S1. Crystal data and structure refinement parameters for ligand and **YCR**

	H_2L	**YCR**
Empirical formula	$C_{13}H_9N_3O_2$	$C_{28}H_{19}Cu_2I_{0.4}N_9O_{10.2}$
Formula weight	239.23	822.56
Crystal system	Triclinic	Cubic
Space group	*P*-1	*Fd*-3*c*
a (Å)	15.9978(7)	43.0555(2)
b (Å)	20.7757(9)	43.0555(2)
c (Å)	20.8014(11)	43.0555(2)
α (°)	112.317(4)	90
β (°)	91.861(4)	90
γ (°)	92.070(4)	90
V ($Å^3$)	6383.6(5)	79815.3(6)
Z	24	96
Temperature (K)	293(2)	100(2)

D_{calcd} (g/cm^3)	1.494	1.643
GOF	1.039	1.061
R_{int}	0.0325	0.0406
R_1 (all data)[a]	0.0741	0.0763
wR_2 (all data)[a]	0.2282	0.1885
R_1[I >2σ(I)][a]	0.0529	0.0570
wR_2[I >2σ(I)][a]	0.1481	0.1594

[a] $R_1 = \Sigma|F_o| - |F_c||/\Sigma|F_o|$; $wR_2 = \{[\Sigma w(F_o^2-F_c^2)^2]/\Sigma[w(F_o^2)^2]\}^{1/2}$; $w = 1/[\sigma^2(F_o^2) + (aP)^2 + bP]$, where $P = [\max(F_o^2, 0) + 2F_c^2]/3$ for all data.

Table S2. Selected bond lengths (Å) and bond angles (°) for **YCR**

YCR			
Cu1-O2	1.961(4)	Cu1-O1a	1.984(4)
Cu1-N1	2.009(5)	Cu1-N3b	2.016(5)
Cu1-O4	2.364(7)		
O2-Cu1-O1a	86.10(16)	O2-Cu1-N1	91.11(17)
O1a-Cu1-N1	160.68(18)	O2-Cu1-N3b	169.28(18)
O1a-Cu1-N3b	89.25(17)	N1-Cu1-N3b	96.41(19)
O2-Cu1-O3c	80.0(3)	O1a-Cu1-O3c	110.2(4)
N1-Cu1-O3c	88.1(4)	N3b-Cu1-O3c	92.6(3)
O2-Cu1-O4	84.7(2)	O1a-Cu1-O4	80.7(2)
N1-Cu1-O4	118.2(2)	N3b-Cu1-O4	85.1(2)
O3c-Cu1-O4	30.4(3)		

Symmetry transformations used to generate equivalent atoms:
a z,-y+3/4,-x+1/4; b -y+1/2,-x+1/2,-z+1/2; c -x,z+1/4,y-1/4.

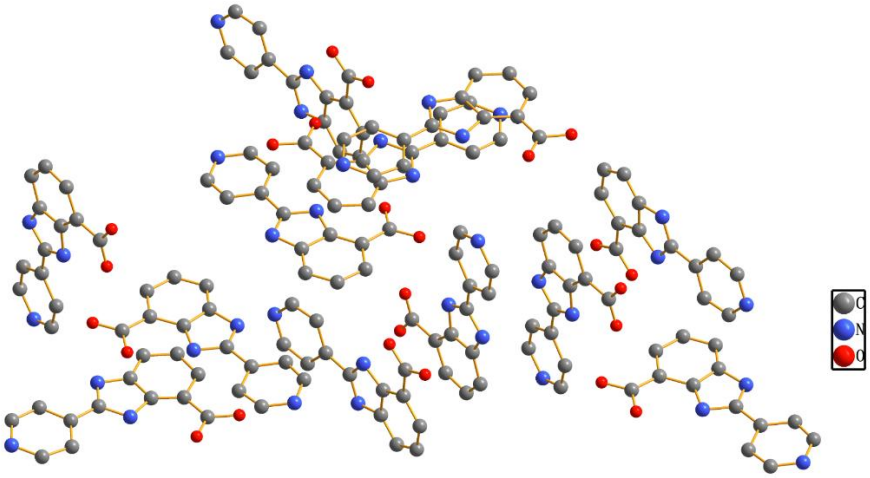

Fig. S4 Crystal packing of the ligand (H atoms are omitted for clarity).

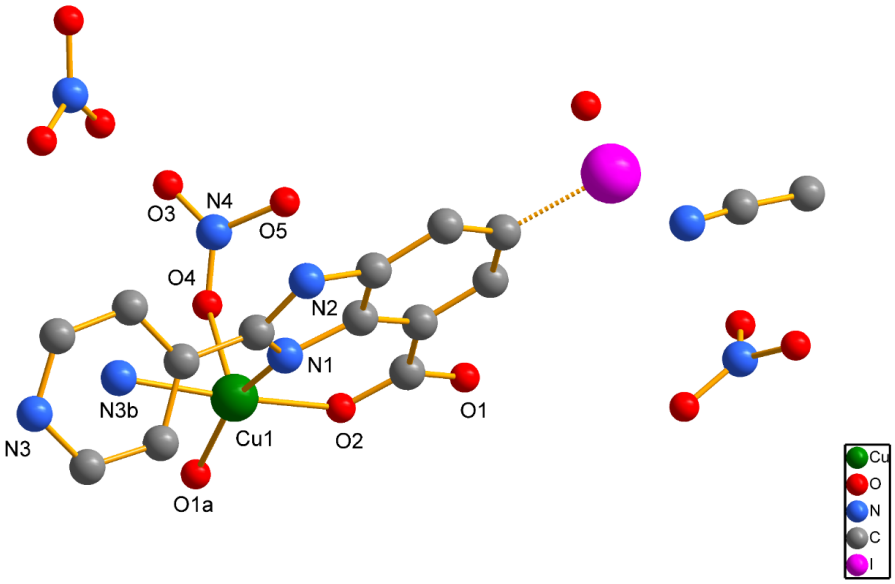

Fig. S5 Coordination environment of **YCR**. One-fifth of H_2L was iodinated, and H atoms are omitted for clarity.

Comment: Note that in situ iodination does not change the charge of the ligand; both the iodinated (HL-I) and uniodinated (HL) ligands have the charge of -1. Without distinguishing iodinated/uniodinated ligand, the formula of YCR before and after the iodination are identical. The bond length of C–I attached to aromatic ring is about 2.10 Å, while in **YCR** the C_{Ph}–I bond length of is about 2.05 Å, which is reasonable to propose in situ iodination of the ligand without affecting the charge balance.[S2,S3]. See Fig. S24-26 for additional characterization for the existed iodine element.

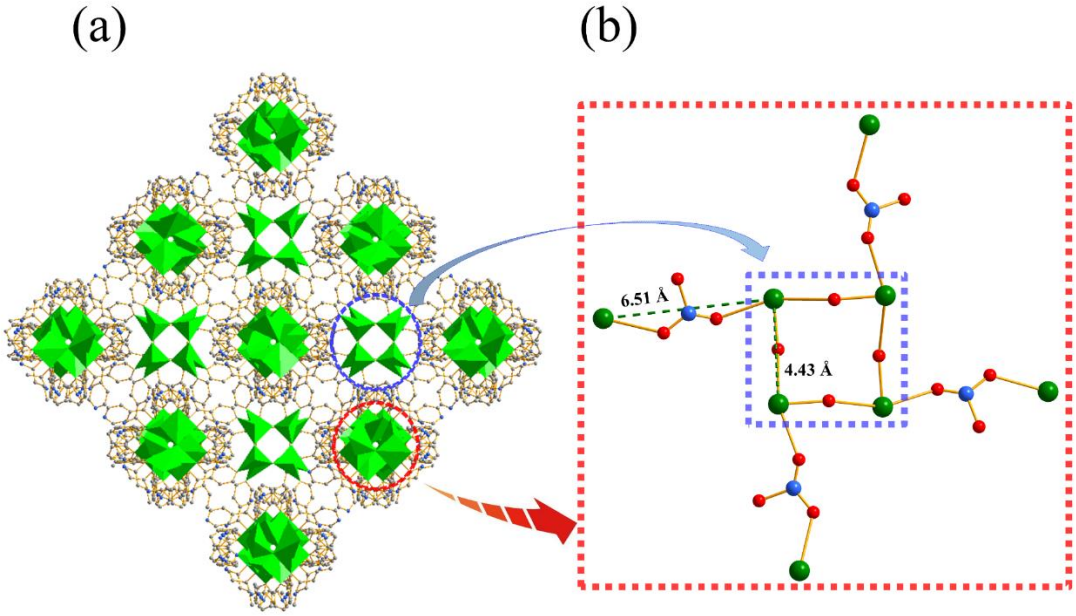

Fig. S6 (a) 3D cationic framework along a/b/c axis in **YCR**. (b) Distance between Cu(II)---Cu(II) and Cu(II)---NO_3^- anion of the tetranuclear Cu_4O_4 cluster (Color codes: green, Cu; red, O; blue, N).

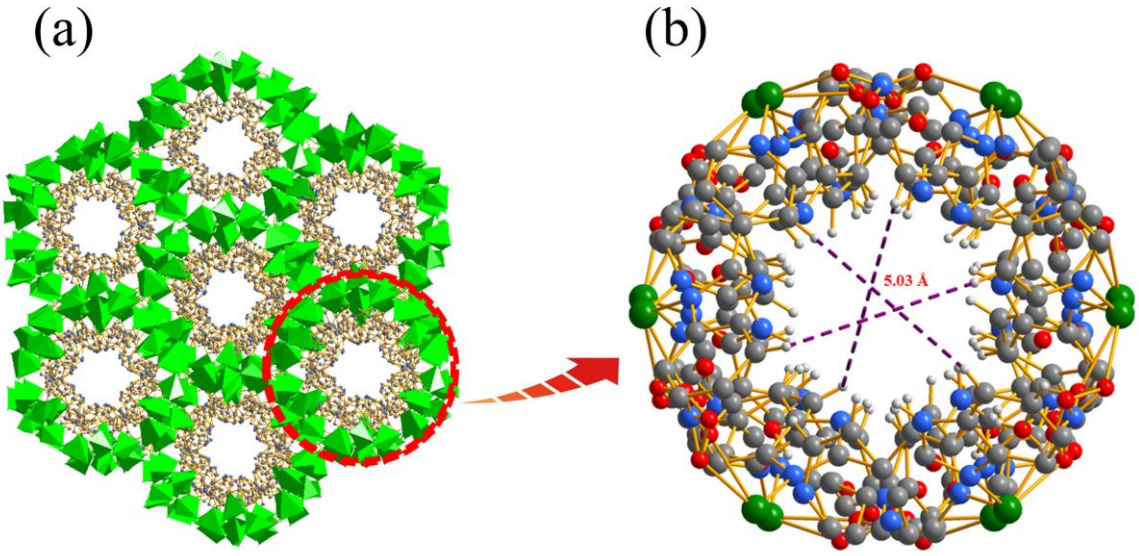

Fig. S7 (a) 3D cationic framework showing 1D channels along [1 1 1] direction in **YCR**. (b) Magnified region of 1D channels (guest molecules and NO_3^- are removed for clarity).

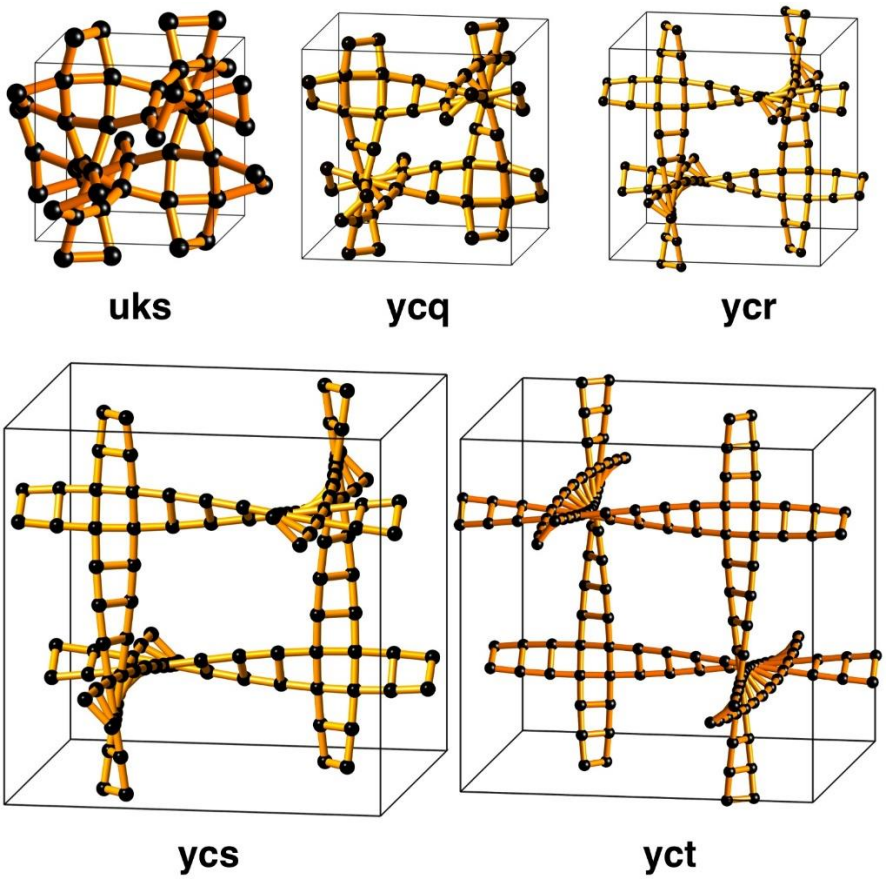

Fig. S8 A family of cubic nets formed from helical ladders, derived from the uninoal 4-coordinated **uks** net.

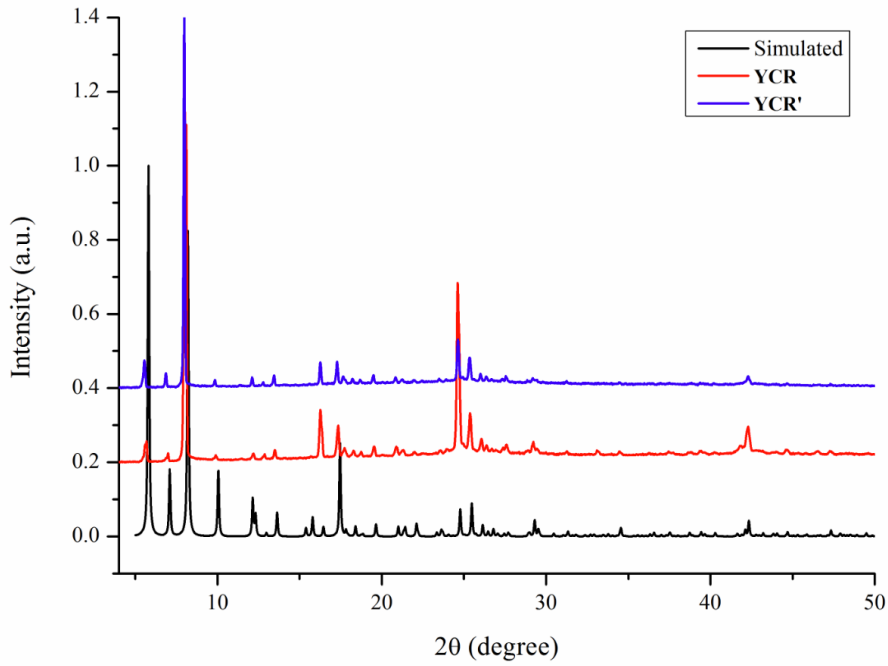

Fig. S9 Simulated and experimental PXRD patterns of **YCR** and **YCR'**.

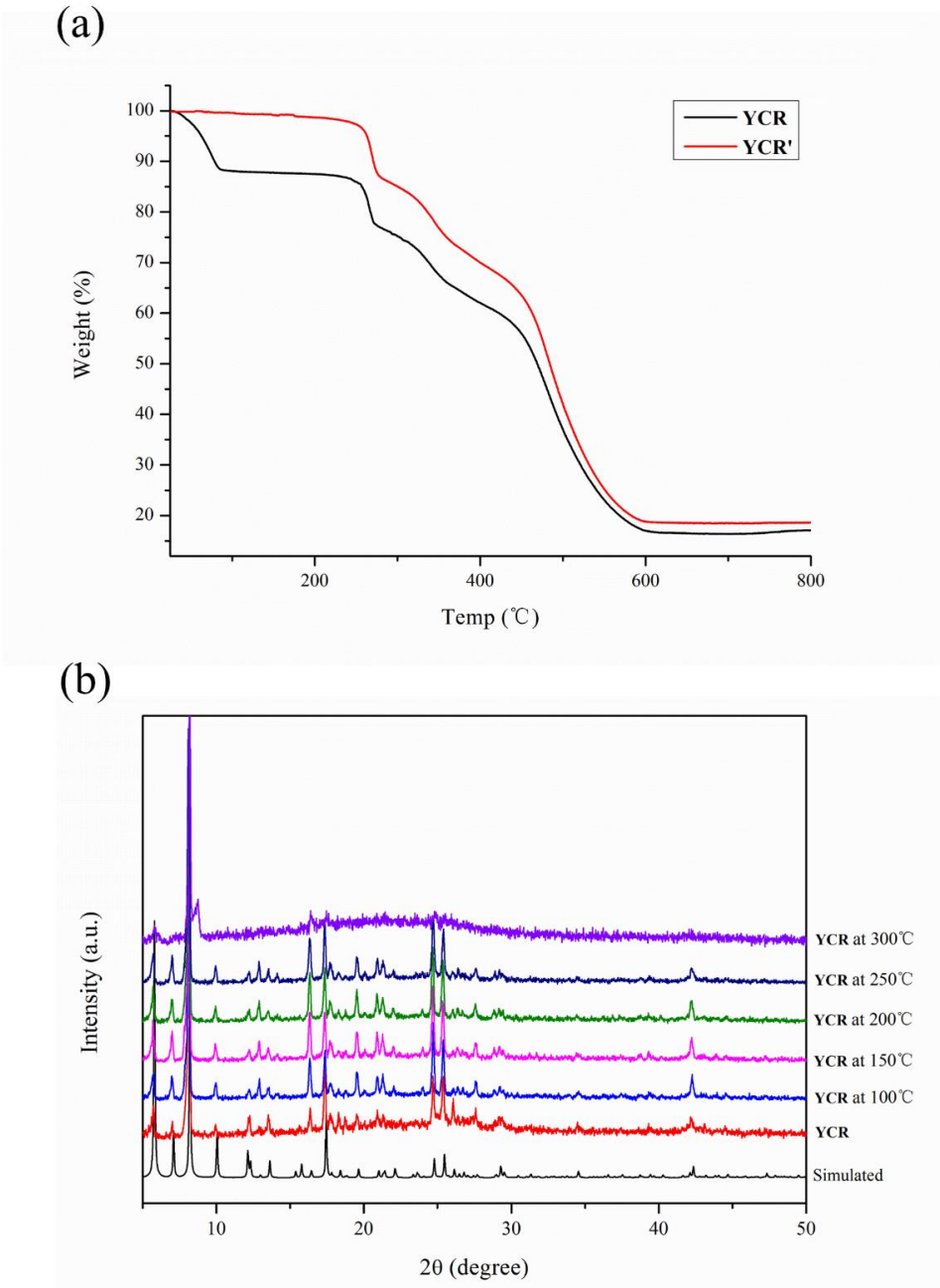

Fig. S10 Thermal stability. (a) Thermogravimetric curves of **YCR** and **YCR'**. (b) Variable temperature PXRD patterns of **YCR**.

Comment: In TGA curves, the weight loss before 90 °C indicates loss of guest water and acetonitrile molecules, whereas weight loss (82%) in the temperature from 250-600 °C relates to decomposition of the framework, with CuO as residue. Additionally, variable temperature PXRD patterns showed that the crystalline phase could be maintained below 250 °C.

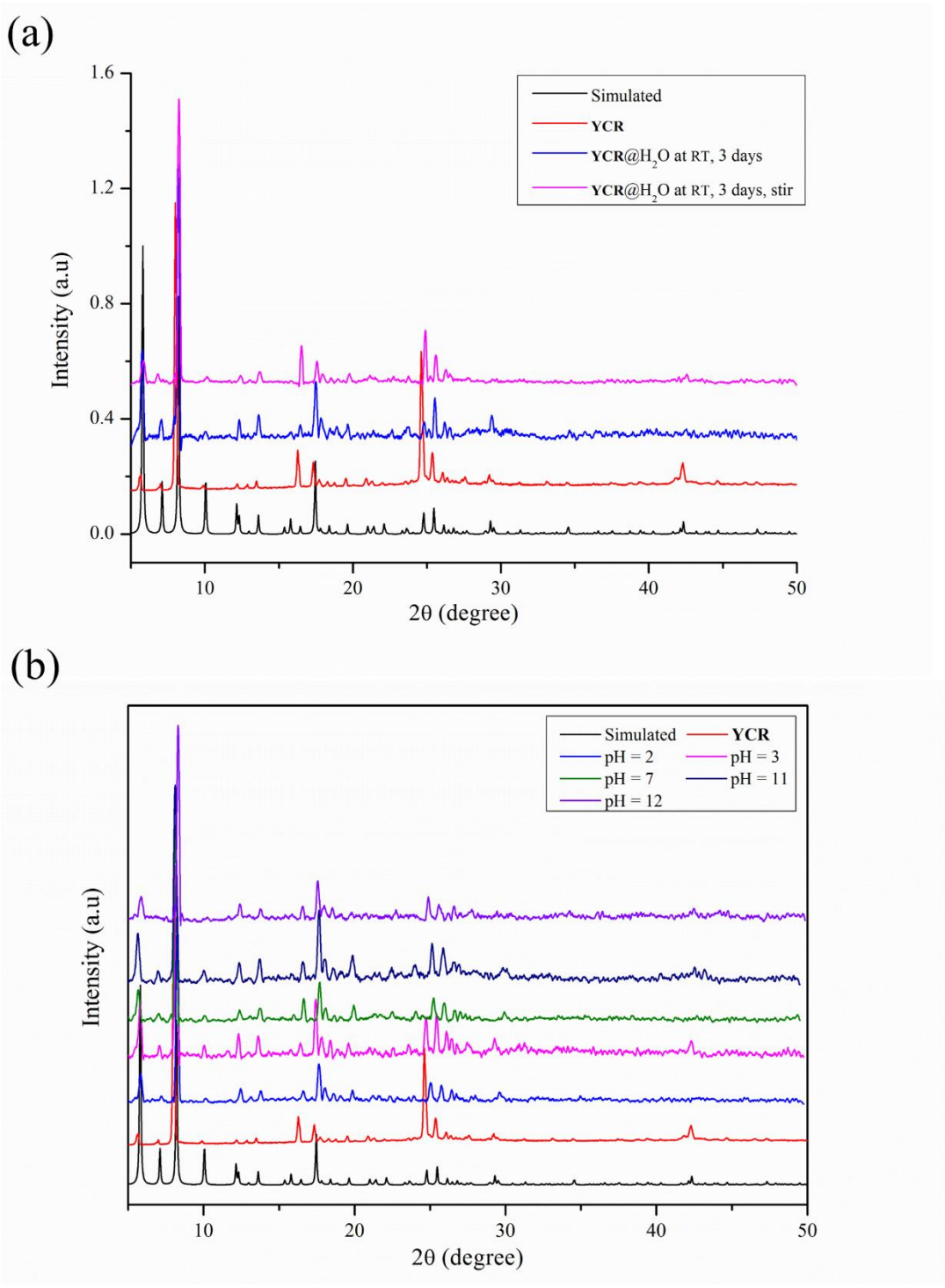

Fig. S11 Chemical stability. (a) PXRD patterns of as-synthesized sample and soaked in water for 3 days. (b) PXRD patterns of as-synthesized sample and after immersion in aqueous solutions of HCl and NaOH at different pH ranging from 2 to 12 for 24 h.

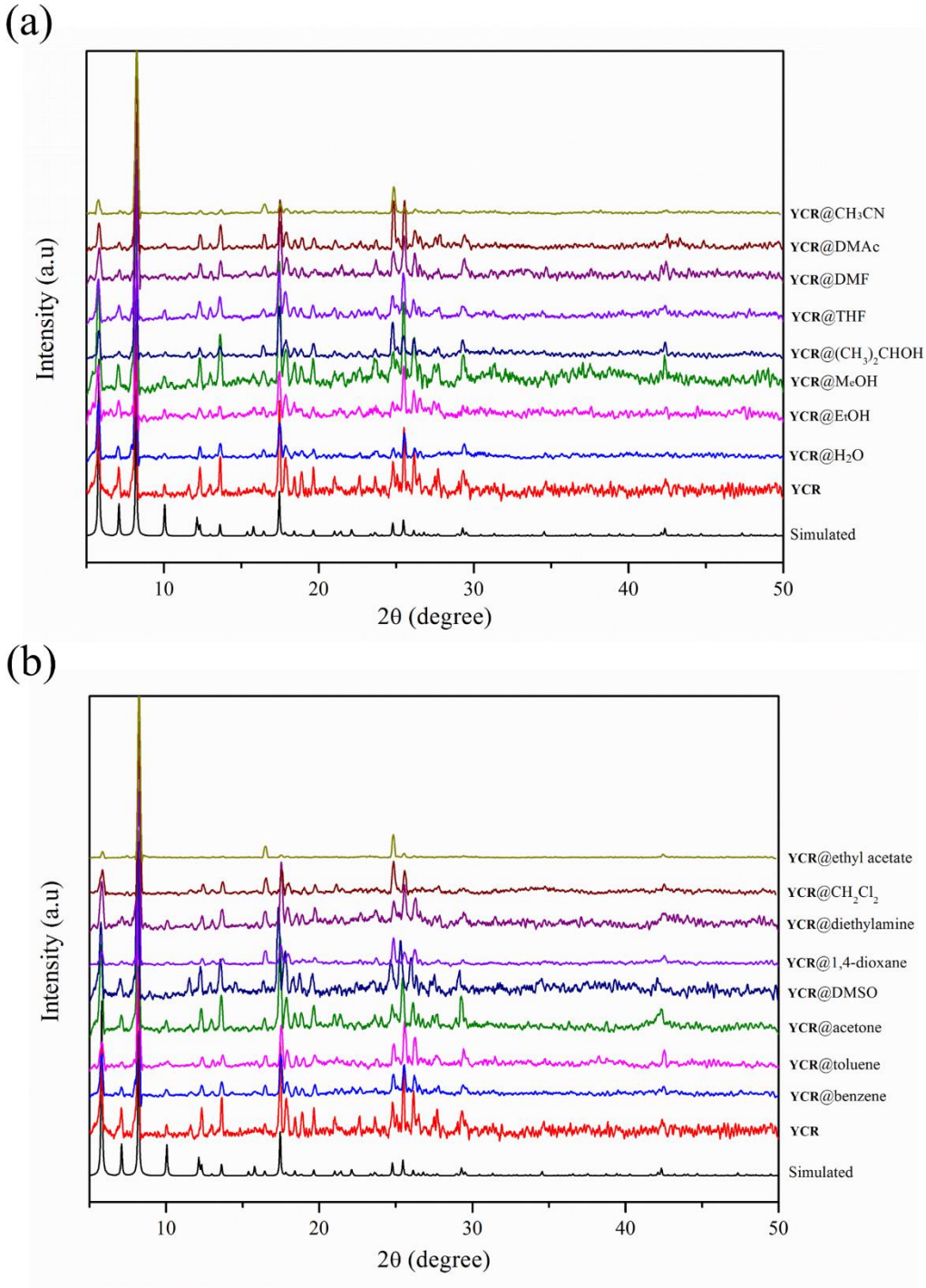

Fig. S12 Solvent stability. (a) (b) PXRD patterns of as-synthesized sample and soaked in different organic solvents for 3 days.

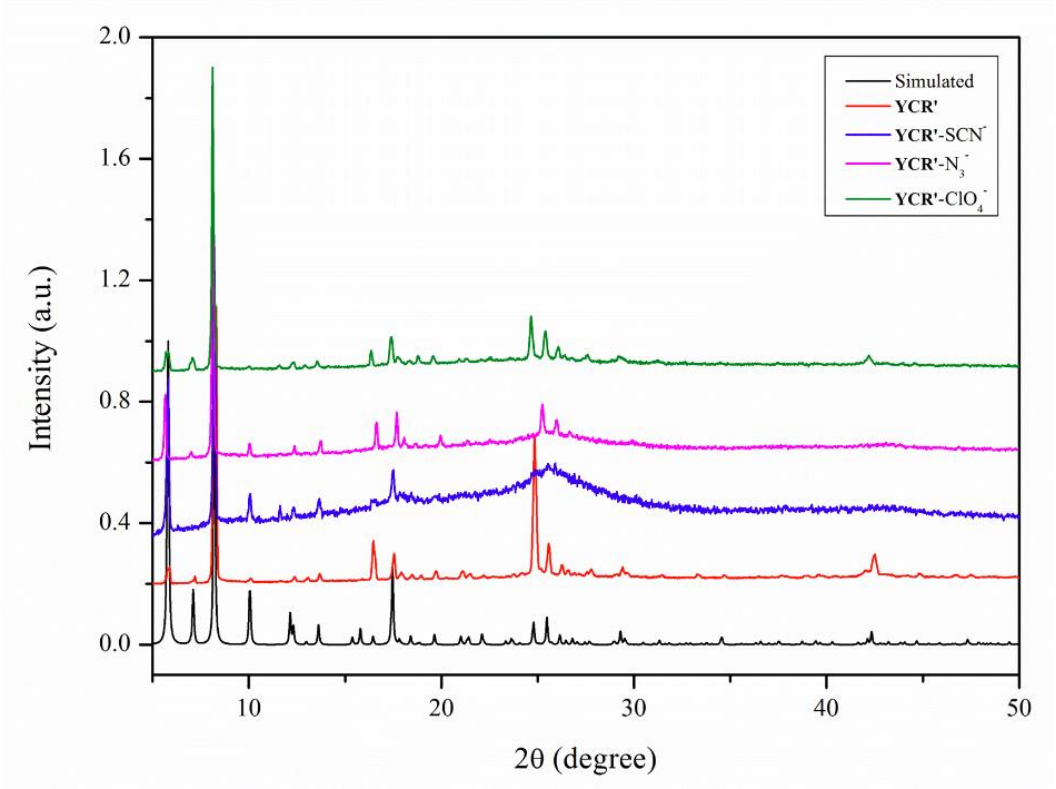

Fig. S13 PXRD patterns of anion-exchanged products, with **YCR′** immersing in aqueous solution of NaN_3, NaSCN and $NaClO_4$, respectively.

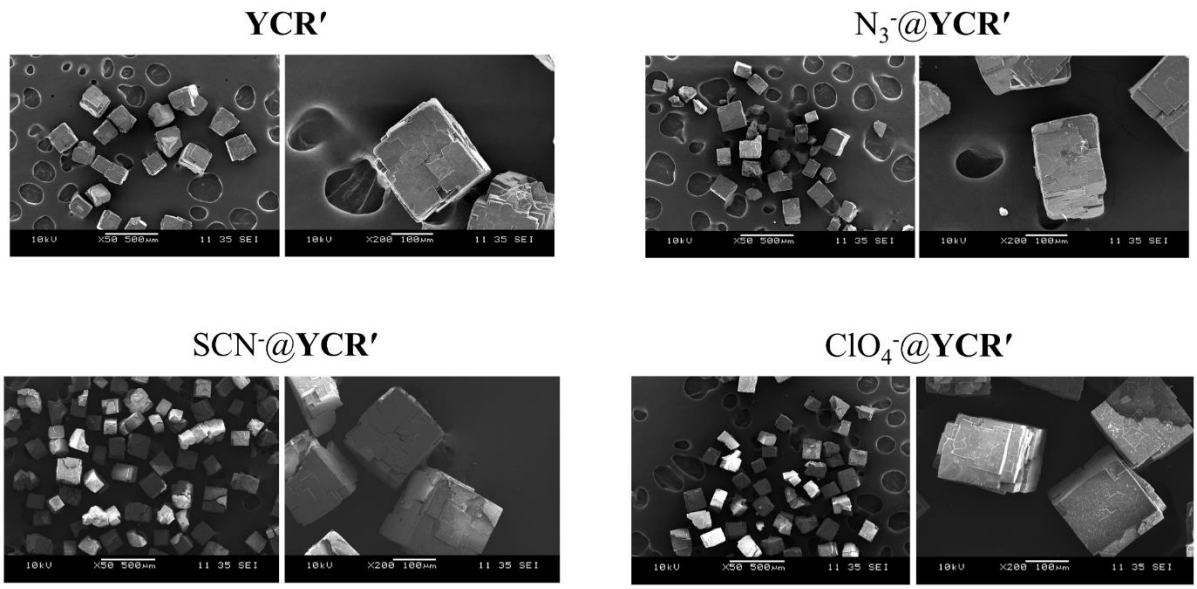

Fig. S14 SEM images of the complex **YCR′** and anion-exchanged products at different magnification.

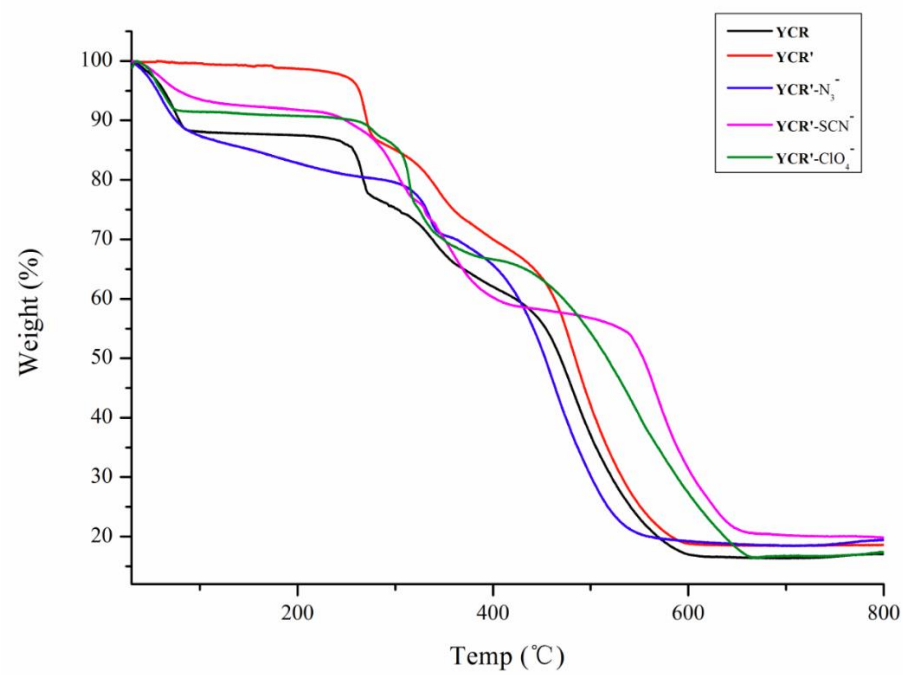

Fig. 15 TGA of **YCR**, **YCR′** and anion-exchanged products.

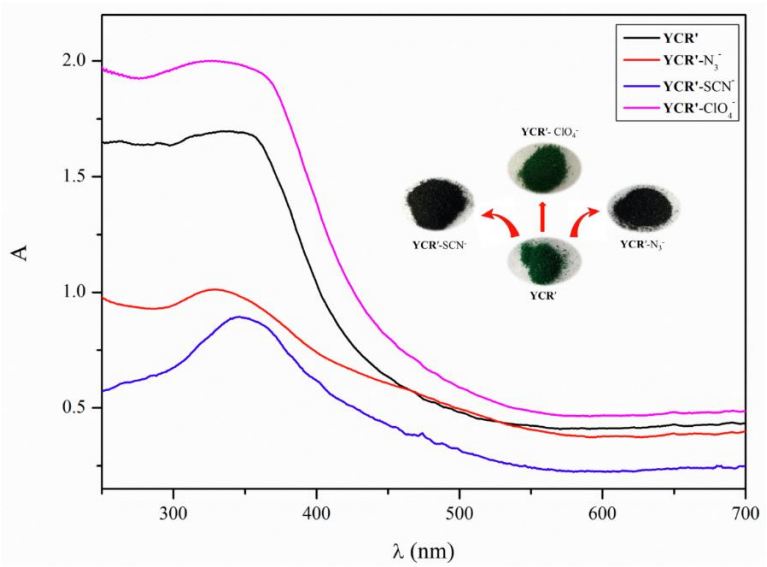

Fig. S16 UV-vis absorption spectra of **YCR′**, **YCR′**-N_3^-, **YCR′**-SCN^- and **YCR′**-ClO_4^-. Inset: the color change was evident to the naked eye within 24 h after capturing different anions.

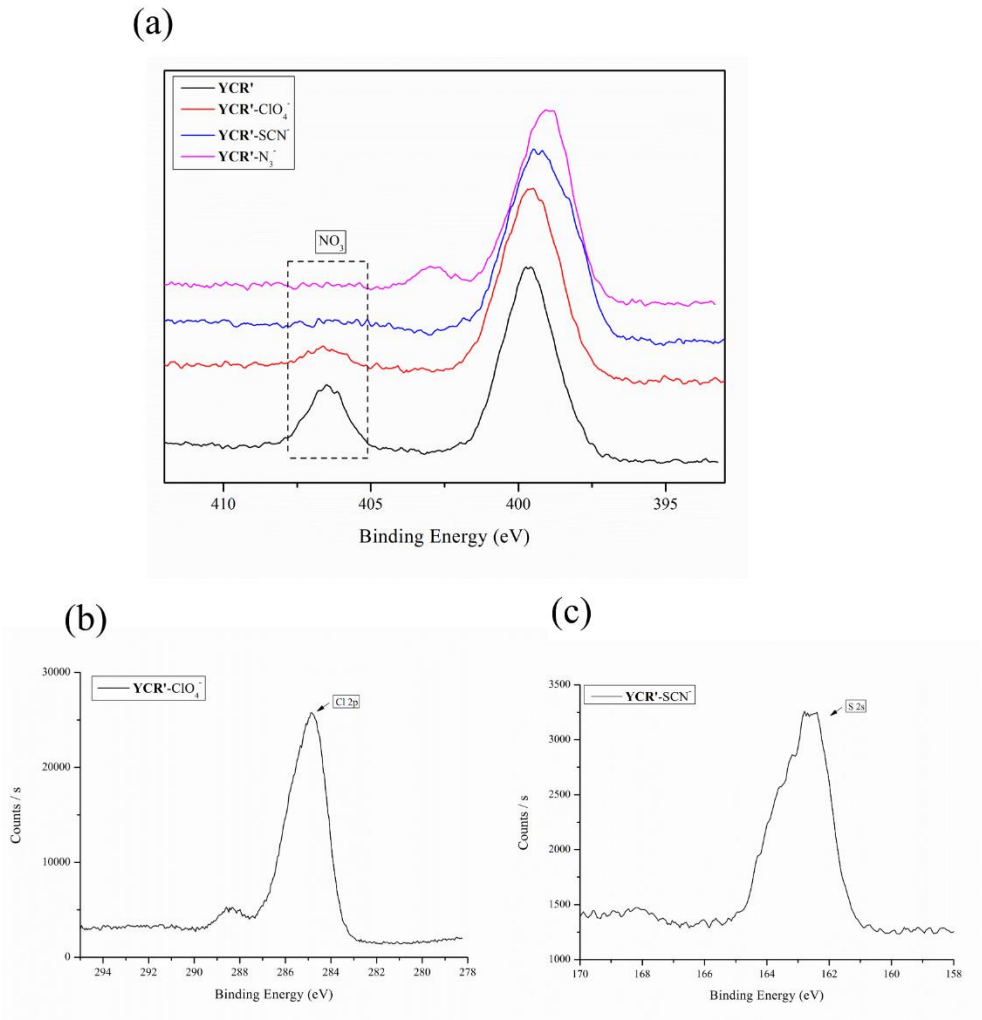

Fig. S17 XPS spectra for determining (a) nitrate species in ion-exchanged **YCR′**, (b) halogens in **YCR′**-ClO_4^-, and (c) sulfur in **YCR′**-SCN^-.

Comment: As shown in Fig. S17a, the N 1s signal of NO_3^- can be found at 407 eV.[S4,S5] The signal intensities of NO_3^- of ion-exchanged materials partly or completely disappeared compared with **YCR**'. Meanwhile, the Cl 2p (285 eV) (Fig. S17) and S 2p (162 eV) (Fig. S17c) peaks[S6,S7] well supported the existence of halogens in **YCR′**-ClO_4^- and sulfur in **YCR′**-SCN^-, respectively.

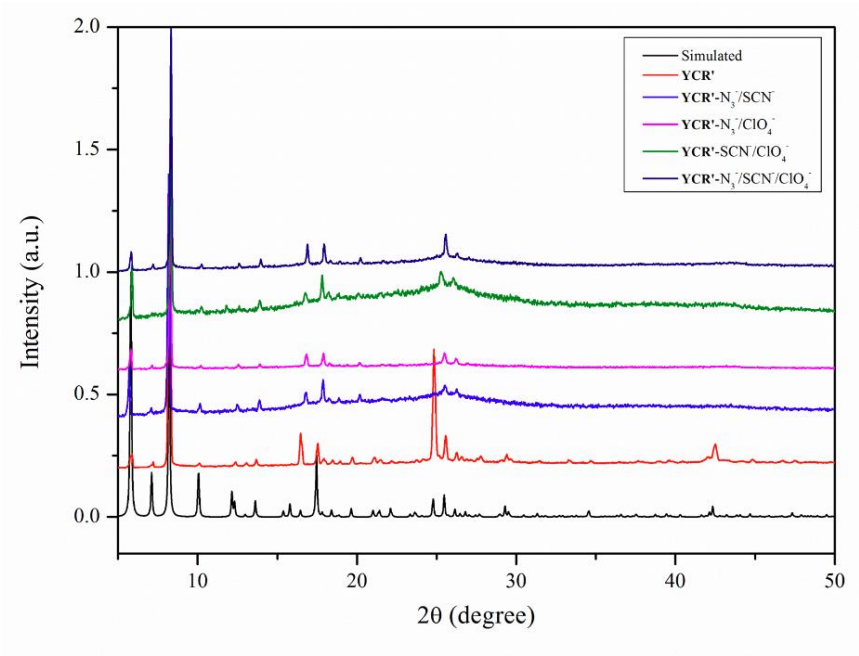

Fig. S18 PXRD patterns of anion-exchanged products, with **YCR′** immersing in aqueous solution of different mixtures of anions.

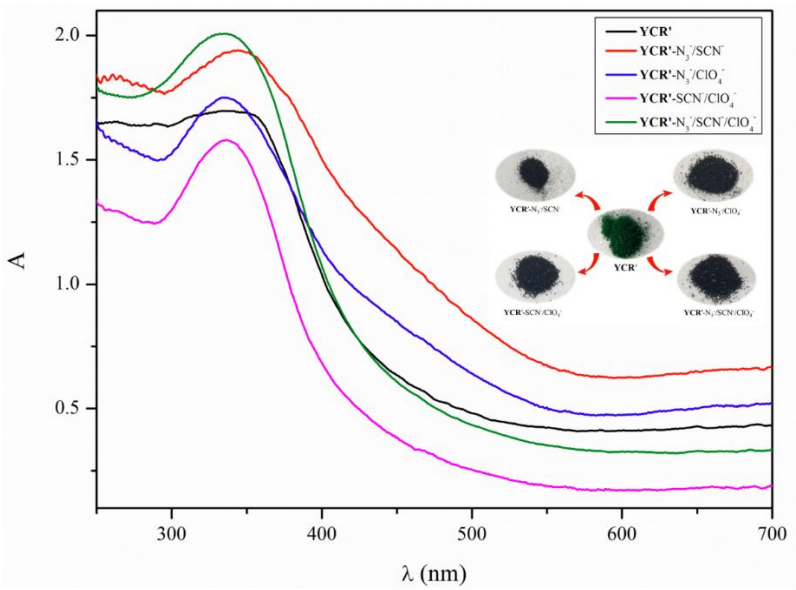

Fig. S19 UV-vis absorption spectra of **YCR′**, **YCR′**-N_3^-/SCN^-, **YCR′**-N_3^-/ClO_4^-, **YCR′**-SCN^-/ClO_4^- and **YCR′**-N_3^-/SCN^-/ClO_4^-. Inset: the color change immersed in different mixed anions.

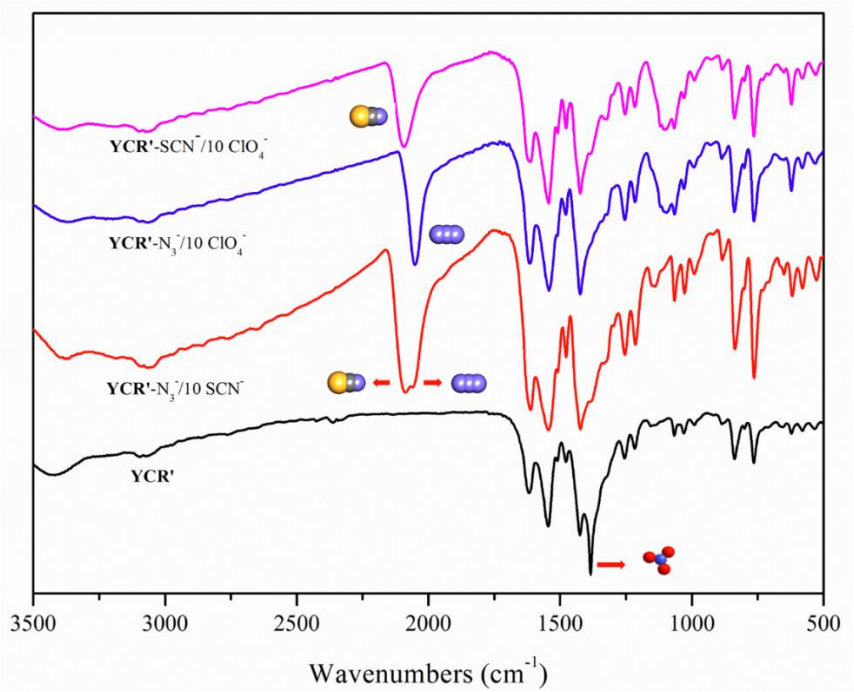

Fig. S20 FT-IR spectra of **YCR′** in different molar ratio among foreign anionic competitors: (N_3^- : SCN^- = 1:10, N_3^- : ClO_4^- = 1:10 and SCN^- : ClO_4^- = 1:10).

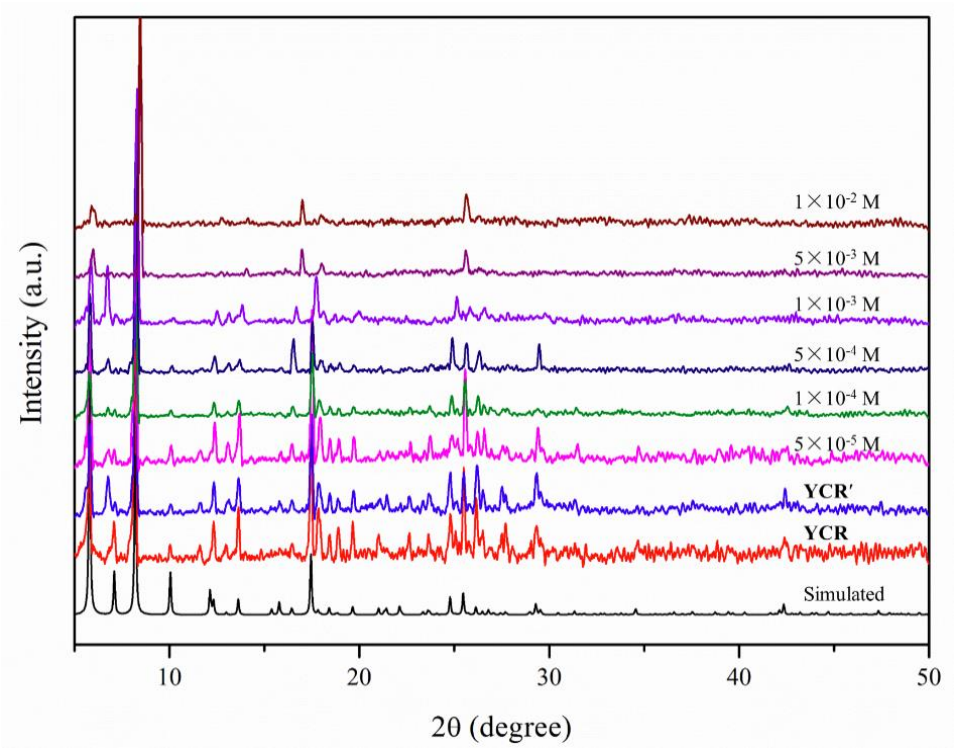

Fig. S21 PXRD patterns of anion-exchanged products, with **YCR′** immersing in aqueous solution of N_3^- anion in the range of 10^{-5}-10^{-2} M for 12 h.

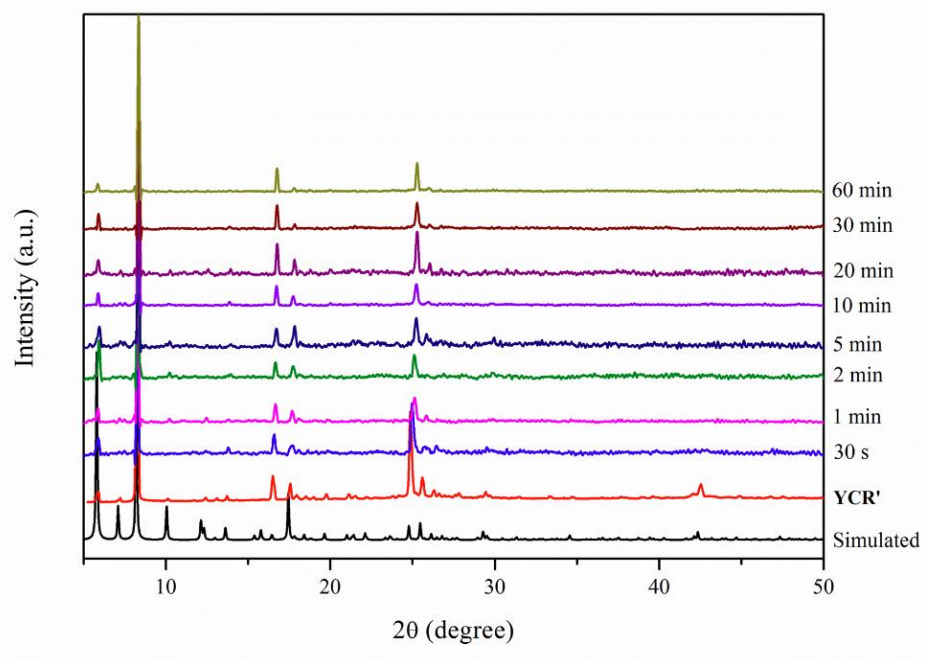

Fig. S22 PXRD patterns of anion-exchanged products, with **YCR′** immersing in aqueous solution of N_3^- anion (10^{-2} M) for different time (within 1 h).

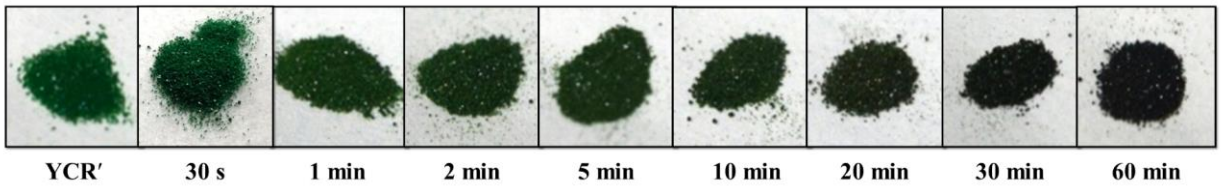

Fig. S23 Images of crystals showing the color deepening upon immersing **YCR′** in 10^{-2} M aqueous solution of N_3^- anion for different time (within 1 h).

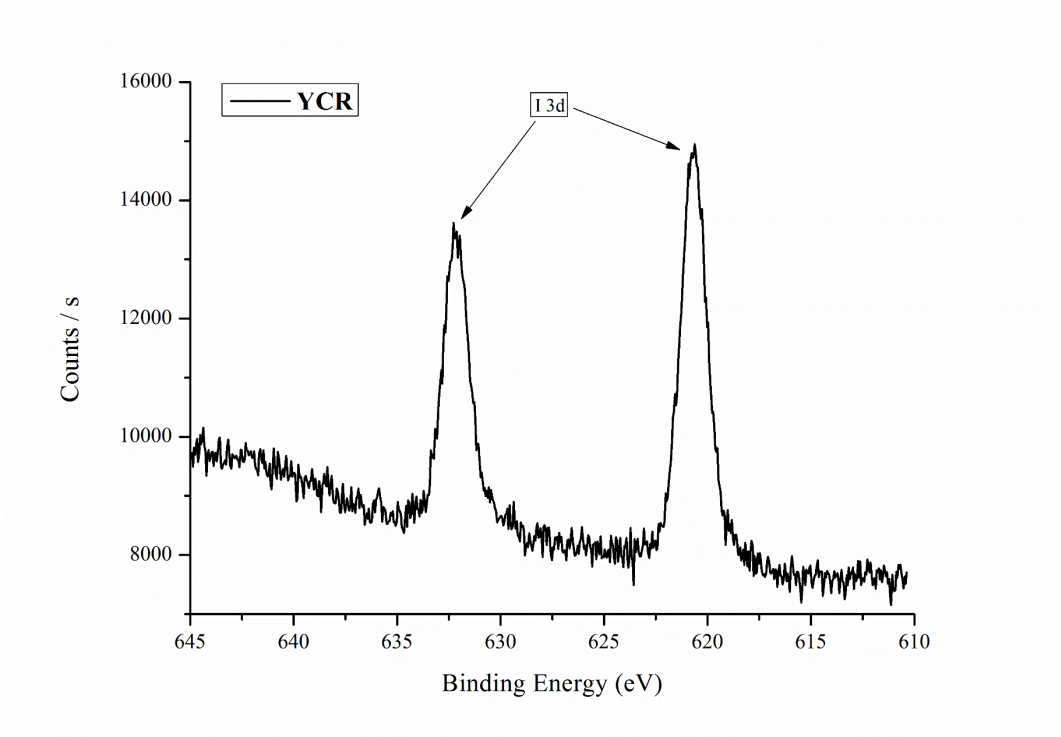

Fig. S24 XPS spectrum of **YCR**, which shows the presence of iodine.

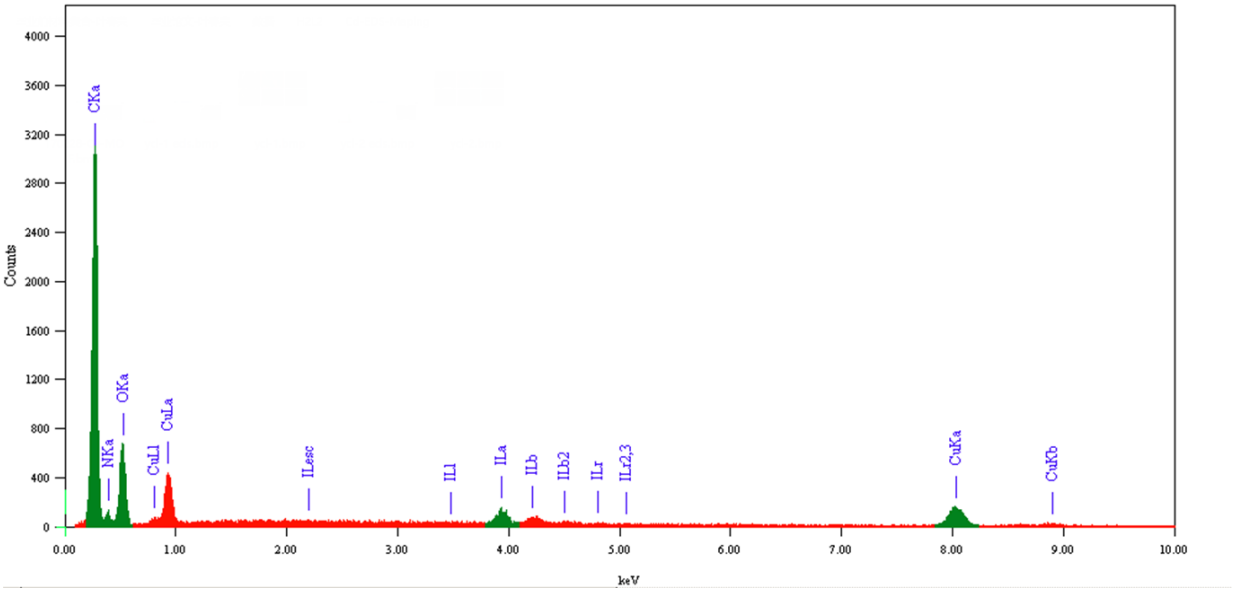

Fig. S25 SEM-based EDS spectrum of **YCR**.

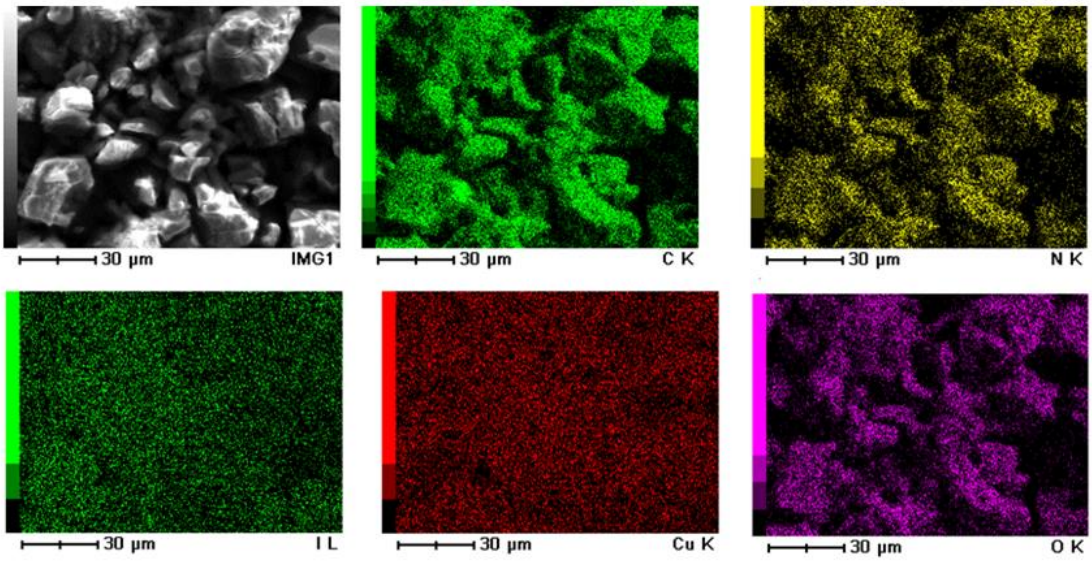

Fig. S26 SEM-based element mapping of **YCR**.

Comment: Additional measurements, such as of XPS (Fig. S24) and SEM-based EDS (Fig. S25) as well as element mapping (Fig. S26) were performed to confirm the existed iodine element in the chemical formula.

References

[S1] G. M. Sheldrick, *Acta Crystallogr. A*, 2008, **64**, 112.

[S2] T. Wu, D. Li and S. W. Ng, *CrystEngComm*, 2005, **7**, 514.

[S3] Y. Zhang, H. Zhang and J. Xiang, *Z. Anorg. All. Chem.*, 2016, **642**, 1173.

[S4] P. Valvekens, D. Jonckheere, T. De Baerdemaeker, A. V. Kubarev, M. Vandichel, K. Hemelsoet, M. Waroquier, V. Van Speybroeck, E. Smolders, D. Depla, M. B. J. Roeffaersa and D. D. Vos, *Chem. Sci.*, 2014, **5**, 4517.

[S5] S. B. Han, D. H. Kwak, H. S. Park, I. A. Choi, J. Y. Park, S. J. Kim, M. C. Kim, S. Hong and K. W. Park, *Angew. Chem. Int. Ed.*, 2017, **56**, 2893.

[S6] Y. Q. Chen, G. R. Li, Z. Chang, Y. K. Qu, Y. H. Zhang and X. H. Bu, *Chem. Sci.*, 2013, **4**, 3678.

[S7] J. P. Ma, Y. Yu and Y. B. Dong, *Chem. Commun.*, 2012, **48**, 2946.